Appl. Phys. A (2015) 118:345–351
DOI 10.1007/s00339-014-8737-0

Applied Physics A
Materials Science & Processing

Polaron activation energy of nano porphyrin nickel(II) thin films

M. Dongol · A. El-Denglawey · A. F. Elhady · A. A. Abuelwafa

Received: 21 April 2014 / Accepted: 13 August 2014 / Published online: 28 August 2014

Abstract 5,10,15,20-Tetraphenyl-21*H*, 23*H*-porphyrin nickel(II), NiTPP films were prepared by thermal evaporation method of mother powder material. Electrical as well as thermo-electric properties were investigated for the as-deposited and annealed NiTPP films. The effect of NiTPP film thickness (160–460 nm) and isochronal annealing in temperature range (300–348 K) on DC electrical properties were studied. Both bulk resistivity and the mean free path were determined; their values are 1.38×10^5 Ω cm and 0.433 nm, respectively. The electrical conductivity exhibits intrinsic and extrinsic conduction. The values of activation energy in extrinsic and intrinsic regions are 0.204 and 1.12 eV, respectively. Mott's parameters were determined at low temperature. Seebeck coefficient indicates *p*-type conduction of NiTPP films. Carrier density, mobility and holes concentration were determined. Seebeck coefficient decreases with the increasing of temperature, while the conductivity increases with the increasing of temperature. The difference between the conductivity and the thermoelectric power activation energies was attributed to the potential barrier grain boundaries.

M. Dongol · A. El-Denglawey (✉) · A. F. Elhady · A. A. Abuelwafa
Nano and Thin Film Laboratory, Physics Department, Faculty of Science, South Valley University, Qena 83523, Egypt
e-mail: denglawey@lycos.com

A. El-Denglawey
Physics Department, Faculty of Applied Medical Science, Taif University, Turabah 21995, KSA

1 Introduction

At the beginning of the twenty-first century, new electronics revolution has become possible due to the development and understanding of a new class of materials, commonly known as organic semiconductors. In this class of materials, the molecular orbitals split into bonding and anti-bonding states. The bonding states are the highest occupied molecular orbitals (HOMO; π-orbitals), and anti-bonding states are the lowest unoccupied molecular orbitals (LUMO; π*-orbitals). This splitting is due to the interaction of adjacent chains along given directions yields the transfer integral to be used for the description of hole (electron) transport in these directions [1–3]. HOMO level is analogous to the term valence band, associated with inorganic semiconductors, and used to imply a lower set of energy levels, completely filled with electrons. Similarly, LOMO level can be compared to the conduction band, a term used to explain a vacant or partially occupied set of many closely spaced electronic levels in which the electrons are free to move [1–3]. The higher the HOMO (LUMO) bandwidth, the higher the expected hole (electron) mobility. It turns out that, at low temperature, the charge transport in a number of organic crystals and highly organized thin films can be described in a band-like regime similar to that in inorganic semiconductors. In that case, the difference or the total widths and shapes of the valence and conduction bands formed by the interaction of the HOMO and LUMO levels of the π-conjugated chains, respectively, determine the hole and electron mobilities or the band gap of the material [1–3].

The enormous progress in this field has been driven by the expectation to realize new applications, such as large area, flexible light sources and displays, low-cost printed integrated circuits or plastic solar cells from these materials

[4]. Organic thin-film transistors (OTFTs), organic light-emitting diodes (OLEDs), photo-sensitive dyes in photovoltaic cells and receptors in chemical gas sensors [5] also, owing to its unique optoelectrical property, porphyrin films offer the promise of widespread adoption in numerous technology areas, including molecular wire [6], information storage [7], nonlinear optical material [8, 9] and optoelectronic devices. The main advantages of using organic materials lie in cost and processability [10, 11].

Characterizations of thin organic semiconductor films are important for pure and applied sciences because of their potential use in electronics and instrumentation industry.

The porphyrins are a class of naturally occurring macrocyclic compounds, which play a very important role in the metabolism of living organisms. The major characteristics of the porphyrin ring are its thermal and chemical stability, coupled with its extensive redox chemistry [12, 13]. The aromatic ring structure can be electrochemically oxidized and/or reduced [14]. Porphyrins have attracted wide research interest, including that of electrochemists, because of their ability to act as electron transfer mediators [15]. As well, porphyrin-based compounds have shown promising properties to use in molecular electronics and as supramolecular building blocks because they spontaneously self-assemble at room temperature on a variety of surfaces. Their limitless functionalization options make it possible to build an assembly with a chosen structure and a wide range of characteristics. There are many available techniques to prepare metalloporphyrins films [16–20]. Thermal evaporation technique was used to prepare 5,10,15,20-tetraphenyl-21*H*,23*H*-porphyrin nickel(II), NiTPP films. NiTPP nanostructure properties were studied through our earlier work [21, 22]. To the author's knowledge, no such information is available in the literature for DC electrical conductivity and thermoelectric power of thin NiTPP films. The goal of this study was focusing on the electrical properties of NiTPP films.

2 Experimental

Aldrich powder NiTPP was used to prepare NiTPP films as received condition. Edwards coating unit model E-306A was used to prepare NiTPP films with different thicknesses (160–460 nm) by direct thermal evaporation method in a vacuum of 10^{-6} torr onto clean glass substrates. The evaporation rate was kept constant using a low rate about 0.5 nms^{-1} approximately. Two-point probes technique was used to study the electrical properties of NiTPP films. The results of the electrical measurements were obtained using planar configuration with Au electrodes separated by 5 mm. Films were stored in a dry, nonoxidizing atmosphere. DC electrical conductivity of NiTPP films was obtained by measuring the resistance of mentioned films as a function of temperature within range (300–450 K) using a Keithley 614C instrument. Chromel–Alumel thermocouple monitored by a micro-voltmeter was used as temperature sensor recorder controlled by electric heater.

The resistivity was calculated according to:

$$\rho = R\frac{Wd}{L} \tag{1}$$

where W, d and L are the width, the thickness and the length of the film. More details of the evaporation process and film thickness measurements are available at [23]. Two techniques are available to measure thermoelectric properties, the integral and the differential method. Among those two available techniques, differential technique is applied to study the thermoelectric properties of NiTPP films within temperature range 300–375 K [23, 24]. A temperature difference of about 10 K was maintained across the sample. Planar configuration with Cu electrodes separated by 5 mm with different thicknesses (160–370 nm) was used to measure Seebeck voltage using Keithley electrometer model 614C. The tolerance of the film thickness is about ±2 % and for the resistivity and Seebeck voltage to be ±1 %.

3 Results and discussion

3.1 DC electrical conductivity

3.1.1 Thickness effect

Figure 1 shows the dependence of the resistivity ρ of the as-deposited NiTPP films on the film thickness d calculated according to Eq. 1. It is shown that, the decreasing of dark electrical resistivity with the increasing of the film thickness is nonlinear. This behavior agrees well with the film growth mechanism. Due to the increasing of the film thickness, microstrain decreases because of the decreasing of the lattice defects, which were pronounced at small thickness [25]; this results in a decrease of the film resistivity. This decrease is continuing up to reach relatively thicker film where the film structure resembles that one of bulk material [26]. At such thickness, the film resistivity is equal to that of bulk material, ρ_B. According to Tellier's [27] model of effective mean free path, which takes into account the surface scattering in addition to bulk scattering, the resistivity ρ_f of the film of thickness, d, can be represented by the following relation [28, 29]:

$$\rho_f = \rho_B\left[1 + \frac{3l_o(1-p)}{8d}\right] \tag{2}$$

where ρ_B is the bulk resistivity, l_o is the bulk electron mean free path and p is the specularity parameter, which gives

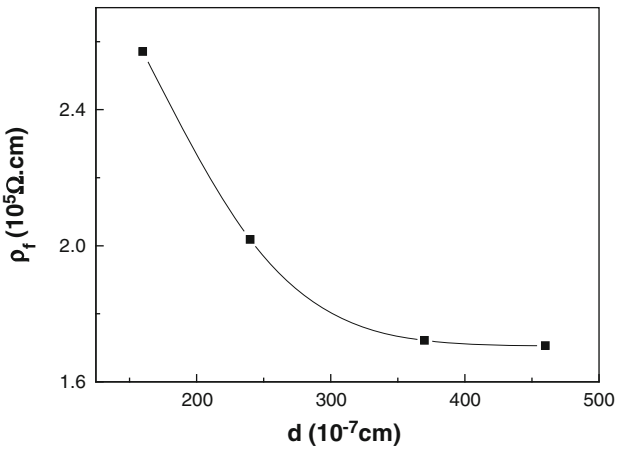

Fig. 1 Dependence of dark resistivity of as-deposited NiTPP films on the film thickness

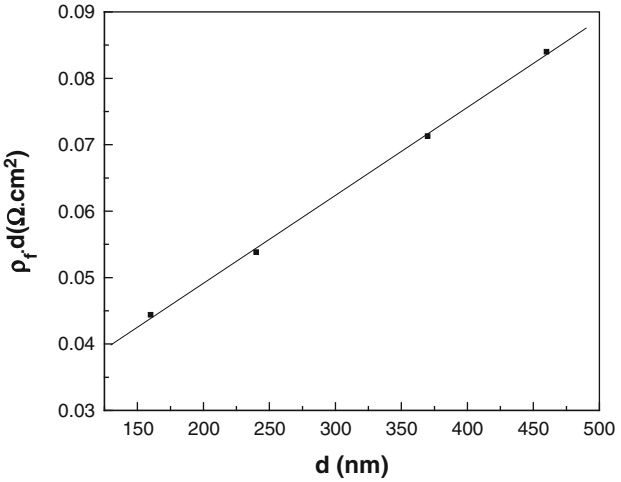

Fig. 2 Variation of $\rho_f \cdot d$ against film thickness of as-deposited NiTPP films

the fraction of electrons incident on the surface that are specularity scattered. This equation is valid only at certain limiting conductions, i.e., large film thickness and/or small mean free path. However, in our case, if we assume a complete diffuse scattering ($p = 0$), Eq. 2 could be rewritten as follows:

$$\rho_f = \rho_B \left[1 + \frac{3}{8} \cdot \frac{l_o}{d}\right] \tag{3}$$

$$\rho_f \cdot d = \rho_B \cdot d + \frac{3}{8} l_o \rho_B \tag{4}$$

According to last two equations, $\rho_f \cdot d$ is a function of the film thickness. The linear relation of $\rho_f \cdot d$ against film thickness of as-deposited NiTPP films is shown in Fig. 2. The slope of the line gives the bulk resistivity, ρ_B, and the intercept of each line gives the mean free path l_o. Figure 2 shows that $\rho_B = 1.38 \times 10^5\ \Omega$ cm and $l_o = 0.433$ nm.

3.1.2 Temperature effect

The temperature dependence of DC electrical conductivity, σ, obeys the well-known Arrhenius Eq. [30]:

$$\sigma = \sigma_o \exp\left(\frac{-\Delta E}{k_B T}\right) \tag{5}$$

where σ_o is the pre-exponential factor, ΔE is activation energy and k_B is Boltzmann's constant. The Arrhenius plot $\ln(\sigma)$ versus (1,000/T) yields a straight line, with a slope corresponding to the value of thermal activation energy. In Fig. 3, $\ln(\sigma)$ versus (1,000/T) is plotted for NiTPP films with different film thicknesses (160–460 nm). According to Davis and Mott [30], the conductivity exhibits different behavior in various regions of the Arrhenius plot. There are two linear regions, first region included within temperature range 300–330 K and the second one in the temperature

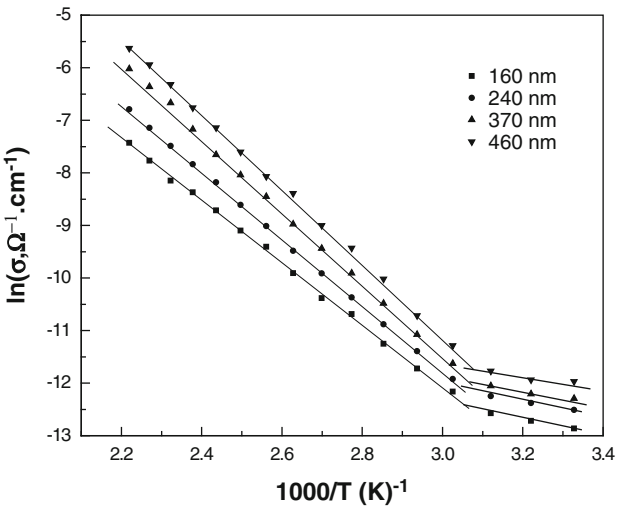

Fig. 3 DC conductivity of NiTPP film as a function of reciprocal temperature for different film thicknesses

range 330–448 K; this yields two activation energies, for extrinsic ΔE_{ex} and for intrinsic ΔE_{in}. The calculated average activation energy in extrinsic region is 0.204 eV and in intrinsic region is 1.12 eV, which approximately is half the onset bandgap of NiTPP ($E_{gopt} \approx 2\ \Delta E_{in} \approx 2.17$ eV) [21]. The conduction mechanism at lower temperatures is explained in terms of hopping through a band of localized states and at higher temperatures in terms of thermal excitation of carriers to the band edges. The slope changes, and hence, the change of the activation energy reflects a change from intrinsic conduction to the extrinsic one [31, 32]. The values of activation energies and the pre-exponential factor are listed in Table 1. Variable range hopping (VRH) conduction mechanism within intrinsic region

Table 1 The values of activation energies ΔE_{in} and ΔE_{ex} for different thicknesses of as-deposited NiTPP thin film

Film thickness (nm)	Intrinsic region		Extrinsic region	
	ΔE_{in} (eV)	σ_{oin} $(\Omega\ m)^{-1}\times10^{3}$	ΔE_{ex} (eV)	σ_{oex} $(\Omega\ m)^{-1}\times10^{-4}$
160	1.02	0.316	0.241	2.73
240	1.10	1.562	0.217	2.44
370	1.18	9.365	0.195	1.97
460	1.19	17.27	0.165	1.50

(300–330 K) takes place through localized states near the Fermi level.

The plot of $\ln(\sigma T^{1/2})$ versus $T^{1/4}$ is shown in Fig. 4. According to VRH model, long hops of carriers from one site to the other one becomes more likely to occur at low temperatures than the sum of all other auxiliary hops. This VRH model is characterized by Mott's [33–35] expression:

$$\sigma(T) = \sigma'_o T^{-1/2} \exp\left(-AT^{-1/4}\right); \tag{6}$$

$$A^4 = T_o = \lambda\alpha^3/k_B N(E_f) \tag{7}$$

where $\lambda = 16$–18 is a dimensionless constant, k_B is Boltzmann's constant, $N(E_f)$ is the density of localized states at E_f, α^{-1} is the spatial extension of the wave function associated with the localized states and T_o is the degree of disorder. The value of σ'_o obtained by various workers [36, 37] is given by:

$$\sigma'_o = 3e^2\gamma[N(Ef)/8\pi\alpha k_B T]^{1/2} \tag{8}$$

where e is the electron charge and γ is the Debye frequency (10^{13} Hz) [38].

Simultaneous solution of Eqs. 6 and 8 yields:

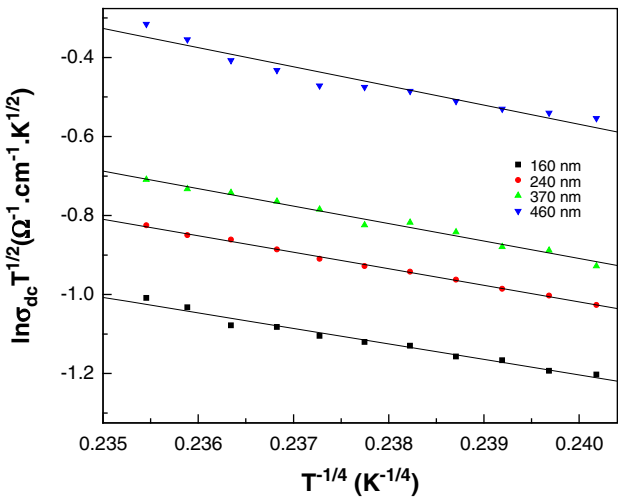

Fig. 4 $\ln\sigma_{dc}T^{1/2}$ versus $T^{-1/4}$ for NiTPP films with different thicknesses

$$\alpha = 22.52\sigma'_o A^2 \text{cm}^{-1} \tag{9}$$

and

$$N(E_f) = 2.12 \times 10^9 \left((\sigma'_o)^3 A^2\right) \text{cm}^{-3}\ \text{eV}^{-1} \tag{10}$$

The hopping distance, R, and the hopping energy, W, are given by [38–40]:

$$R = [9/8\pi\alpha k_B T N(E_f)]^{1/4}\ \text{cm} \tag{11}$$

$$W = [3/4\pi R^3 N(E_f)]\ \text{eV} \tag{12}$$

Various parameters such as density of states $N(E_f)$, degree of disorder T_0, hopping distance R and hopping energy W are called Mott's parameters. These parameters were calculated according to Eqs. 6–12 and listed in Table 2. The values of Mott's parameters W and αR are of the order of the few $k_B T$ and greater than unity, respectively. This shows a close agreement with Mott's VRH [30, 35, 36].

The hopping distance increases with the increasing of the film thickness, while the hopping energy is vise versa. These results are in complete agreement with the concept of VRH.

3.2 Thermoelectric power

The differential category was chosen from the two essential categories techniques of thermoelectric power to study NiTPP films [41]. The thermoelectric power of semiconductor is about 10^3 times that of metals [42]. Copper is used as conducting electrode because the thermoelectric power of copper electrode could be neglected. This means that the measurement of the relative thermoelectric power between NiTPP films and copper as reference is nearly the absolute value of the thermoelectric power of NiTPP films. The hopping of holes at one energy level is given by [43, 44]:

$$S(T) = \frac{-k_B}{e}\left[\frac{E_f - E_\mu}{k_B T} + A_\mu\right] \tag{13}$$

where S is Seebeck coefficient, E_f is the energy of Fermi level, E_μ is the energy of the transport state and A_μ is a constant [44]. The Seebeck coefficient directly reveals (1) the conduction type (n or p transport) by its sign and (2) the energy difference between the Fermi level and the transport state labeled as E_μ. The variation of Seebeck coefficient of NiTPP films with temperature is shown in Fig. 5, which reveals that the value of S is positive over the entire temperature range.

The positive value of Seebeck coefficient indicates p-type conduction of NiTPP, i.e., the conduction is due to holes moving in the valence states of the matrix molecules and not by a hopping of electrons between acceptor states.

Table 2 Mott's parameters for as-deposited NiTPP thin films of different thickness

d (nm)	$T_o \times 10^6$ (K)	$N(E_f) \times 10^{13}$ (eV^{-1} cm^{-3})	$\alpha \times 10^4$ (cm^{-1})	$R \times 10^{-4}$ (cm)	W (meV)	$R\alpha$
160	1.46	5.38	7.51	2.23	40	16.74
240	0.46	1.65	3.45	3.64	29	12.55
370	0.18	0.71	1.93	5.22	23	10.07
460	0.09	0.17	0.94	8.87	19	8.33

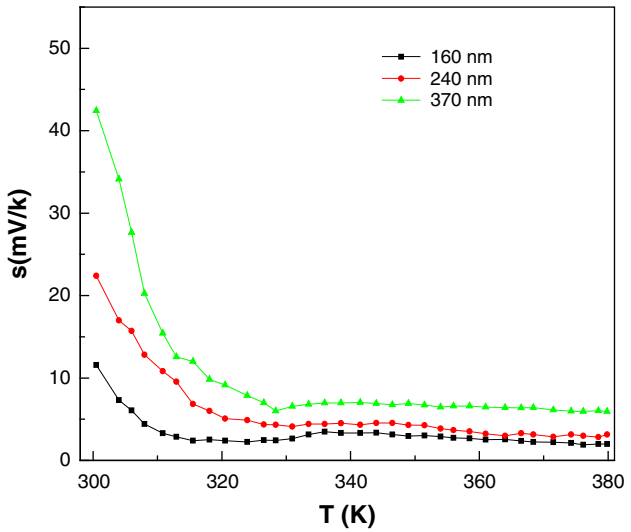

Fig. 5 The variation of Seebeck coefficient S of NiTPP thin films, against temperature, T

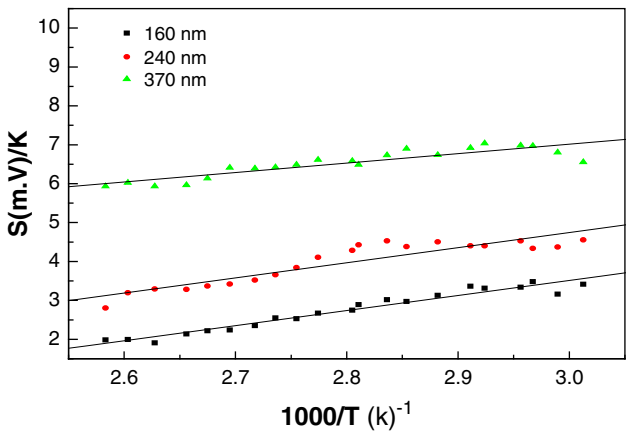

Fig. 6 The variation of Seebeck coefficient S of NiTPP thin films, against 1,000/T

S is continuously decreasing with temperature, indicating a negative shift of the Fermi level E_f toward the transport level E_μ. The general behavior of the conductivity and Fermi level follows the situation of inorganic semiconductors [45]. By combining Seebeck and conductivity results, carrier density and the mobility could be determined. The only assumption in this analysis is that the effective density of states N_μ at the transport level E_μ is comparable to the density of molecules, provided each molecule contributes one state. The hole density can then be directly calculated from the Seebeck coefficient, neglecting A_μ and taking into account that the Maxwell–Boltzmann approximation is justified since; $(E_f - E_\mu) \gg (k_B T)$ [45]. The concentration of holes, p, was calculated from:

$$p = 2\left(\frac{2\pi m^* k_B T}{h^2}\right)^{3/2} \exp\left(\frac{\Delta E}{k_B T}\right) \tag{14}$$

where m^* is the effective mass of charge carrier and ΔE is the thermal activation energy obtained from temperature dependence of resistivity. The hole mobility μ_h can be deduced by applying Eq. [46]:

$$\sigma_{int} = |e|(n_i \mu_e + p_i \mu_h) \tag{15}$$

$$\sigma_{int} = |e| p_i (\mu_e + \mu_h) \tag{16}$$

$$\sigma_{int} = |e| p_i \mu_h \left(1 + \frac{\mu_e}{\mu_h}\right) \tag{17}$$

$$\sigma_{int} = |e| p_i \mu_h (1 + c) \tag{18}$$

where μ_h is holes mobility, μ_e is electrons mobility and c is the calculated mobility ratio (μ_e/μ_h). p_i is the intrinsic hole concentration. In the intrinsic region, the Seebeck coefficient can be given as [46]:

$$S = \frac{-k_B}{e}\left(\frac{c-1}{c+1}\right)\left[\frac{\Delta E_s}{k_B T} + 2\right] \tag{19}$$

where ΔE_s is the activation energy of the thermoelectric power. It is assumed that the effective mass is equal to the rest mass of the electron and the mean value of the thermal activation energy, which obtained from the resistivity measurements. At room temperature, the calculated p according to Eq. 14 is 5×10^{31} m^{-3}. The value of c could be determined from the intercept and ΔE_s from the slope of the graph of S against $1/T$ in the intrinsic region as shown in Fig. 6.

The mean value of $\Delta E_s = 0.97$ eV, and the mobility ratio c was calculated to be 0.92. $\mu_e > \mu_h$ for semiconductor materials; therefore, $c > 1$. However, c values are

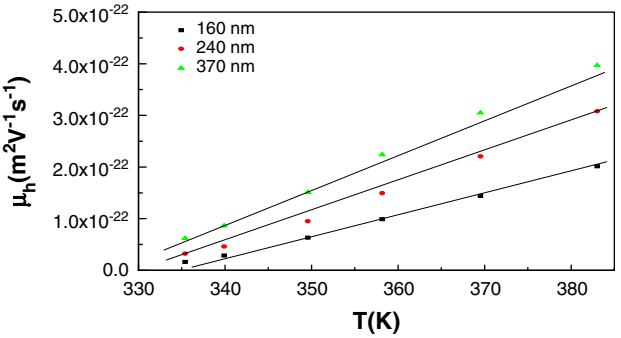

Fig. 7 The calculated holes mobility for NiTPP films as function of temperature, T

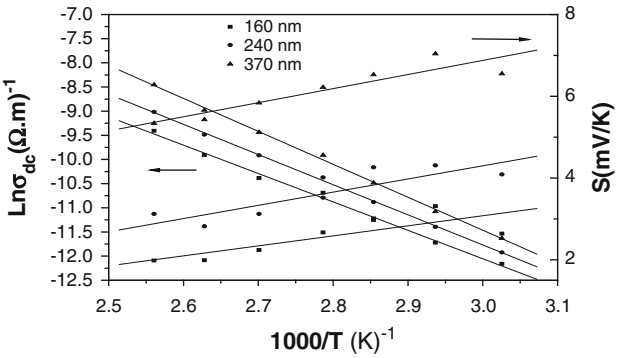

Fig. 8 Variation of S, and $Ln\sigma_{dc}$ versus 1,000/T for as-deposited NiTPP films with different thicknesses

smaller than one have also been given for several inorganic (PbSe, PbTe, etc.) and organic (anthracene, pyrene, etc.) semiconductors [43].

A proposed model is based on band structure representation for explaining these values of the carrier mobility ratio [44]. In this model, the conduction band consists of two overlapping bands. When the electrons are excited from the valence band at lower temperatures, they occupy mainly the lower conduction band, where their mobility is larger than that of the holes. At higher temperatures, the concentration of electrons excited into the upper conduction band increases. At upper conduction band, the electron mobility is smaller than that of the holes [47]; therefore, $c < 1$. According to Eq. 17, Seebeck coefficient of respective semiconductor is positive. According to Eq. 18, the calculated holes mobility of NiTPP films as function of temperature is shown in Fig. 7. Seebeck coefficient S and electrical conductivity σ_{dc} (intrinsic region) as a function of inverse temperature for as-deposited NiTPP thin films of different thickness are depicted in Fig. 8. It is clear that both S and σ_{dc} increase with the increasing of the films thickness, and S decreases with the increasing of temperature, while σ_{dc} increases with the increasing of temperature. The mean value of ΔE_σ was found to be larger than the mean value of ΔE_s. The activation energy of polaron, ΔE_Q, is deduced according to [30]:

$$\Delta E_Q = \Delta E_\sigma - \Delta E_S \tag{20}$$

The calculated value of ΔE_Q is 0.15 eV. In some materials, ΔE_σ was found to be equal to ΔE_s, which has been interpreted in terms of holes conduction in the extended states. In other materials, ΔE_σ was found to be larger than ΔE_s [47–50]. This result may be accounted for either with an intrinsic two carriers model [51] or with conduction by hopping in the valence band with an activation energy for the mobility equal to ΔE_σ–ΔE_s [24, 48–52]. The nonzero value of ΔE_Q is due to the long-range static potential that modulates the energy of the mobility edge in space [53]. The difference between the conductivity and the thermoelectric power activation energies, ΔE_σ–ΔE_s, may also be attributed to a "grain boundary" limited mobility. Since the films are deposited from a vapor, the growth process involves the nucleation and growth of amorphous domains. As these domains grow together, an interface region exists between domains [24]. There are several researches [53–56] reported the existence of voids of approximately 10 Å diameter. If this void network continued to exist in the films, it could serve as a "domain boundary" network that impedes the carrier mobility: ΔE_σ–ΔE_s could then be attributed to the activation energy necessary for carriers to be transported across the voids. One can call the ΔE_σ–ΔE_s as the activation energy of mobility [57], and also, one can suggest that this difference may be due to the potential barrier grain boundaries. Hence, the potential barrier grain boundary plays a distinguishable role in the NiTPP films.

4 Conclusion

Thermal evaporation technique was used to prepare NiTPP films onto clean glass substrates. The as-deposited and annealed samples were considered to investigate the electrical properties within low and high temperature range, while the thermoelectric properties were investigated through the high one only, both as a function of thickness effect. Au was used as conducting electrode to measure the electrical properties. The dark electrical resistivity decreased exponentially with the increasing of the film thickness continuously to reach relatively thicker film. Both bulk resistivity and the mean free path were determined. The electrical conductivity was studied through two temperature ranges: low range 300–330 K and the high one 330–448 K. The intrinsic and extrinsic conductions were revealed for low and high ranges, respectively. VRH conduction was dominated within intrinsic region. The values

of activation energy in extrinsic and intrinsic regions are 0.204 and 1.12 eV, respectively. Mott's parameters: degree of disorder, the spatial extension of the wave function, density of localized states, hopping distance and the hopping energy were determined at low temperature. Copper was used as conducting electrode to measure the thermoelectric properties. Seebeck coefficient indicates *p*-type conduction of NiTPP films. Carrier density, mobility and holes concentration could be determined. The thermoelectric power activation energy was 0.97 eV. Seebeck coefficient and electrical conductivity increase with the increasing of the films thickness. Seebeck coefficient decreases with the increasing of temperature, while the conductivity increases with the increasing of temperature. The difference between the conductivity and the thermoelectric power activation energies was attributed to the potential barrier grain boundaries.

References

1. J.H. Schon, C. Kloc, B. Batlogg, Phys. Rev. Lett. **86**, 3843 (2001)
2. J.L. Bredas, J.P. Calbert, D.A. da Filho Silva, J. Cornil, PNAS **99**, 5804 (2002)
3. N. Lee, H. Shin, Y.J. Kim, C. Kimd, S. Suhd, Rev. Roum. Chim. **55**, 627 (2010)
4. W. Brütting, *Physics of Organic Semiconductors* (WILEY-VCH Verlag GmbH & Co. KGaA, New York, 2005)
5. L. Teugels, *Scanning Tunneling Microscopy Studies of Supramolecular Assemblies of Porphyrins and C60 Fullerenes*, Ph.D. (The University of Chicago, USA, 2009)
6. R.W. Wagner, J.S. Lindsey, J. Am. Chem. Soc. **116**, 9759 (1994)
7. D.T. Gryko, C. Clausen, J.S. Lindsey, J. Org. Chem. **64**, 8635 (1999)
8. X.Q. Zhang, H.M. Wu, Y. Wei, Z.P. Cheng, X.J. Wu, Solid State Commun. **95**, 99 (1995)
9. X.Q. Zhang, H.M. Wu, X.J. Wu, Z.P. Cheng, Y. Wei, J. Mater. Chem. **5**, 401 (1995)
10. A.R. Murphy, J.M.J. Frechet, Chem. Rev. **107**, 1066 (2007)
11. M.M. El-Nahass, A.F. El-Deeb, H.S. Metwally, A.M. Hassaniena, Eur. Phys. J. Appl. Phys. **52**, 10403 (2010)
12. K. De Wael, A. Adriaens, E. Temmerman, Anal. Chim. Acta **554**, 60 (2005)
13. M.M. Makhlouf, A. El-Denglawey, H.M. Zeyada, M.M. El-Nahass, J. Lumin. **147**, 202 (2014)
14. C.C. Leznoff, A.B.P. Lever, *Phthalocyanines, Properties and Applications*, vol. 3 (VCH, Weinheim, 1993), p. 305
15. K. De Wael, P. Westbroek, E. Temmerman, Electroanalysis **17**, 263 (2005)
16. T. Takagi, A. Hoshino, H. Miyaji, K. Izumi, R. Kokawa, Jpn. J. Appl. Phys. **40**, 6929 (2001)
17. A.W. Snow, N.L. Jarvis, J. Am. Chem. Soc. **106**, 4706 (1984)
18. R. Paolesse, C. Di Natale, A. Macagnano, D. Fabrizio, B. Tristano, Sens. Actuators B **47**, 70 (1998)
19. J. Spadavecchia, R. Rella, P. Siciliano, M.G. Manera, A. Alimelli, R. Paolesse, C. Di Natale, A. D'Amico, Sens. Actuators B **115**, 12 (2006)
20. H. Shinmori, T. Kasiwara, A. Osaka, Tetrahedron Lett. **42**, 3617 (2001)
21. M. Dongol, M.M. El-Nahass, A. El-Denglawey, A.F. Elhady, A.A. Abuelwafa, Curr. Appl. Phys. **12**, 1178 (2012)
22. M. Dongol, A. El-Denglawey, A.F. Elhady, A.A. Abuelwafa, Curr. Appl. Phys. **12**, 1334 (2012)
23. A. El-Denglawey Said, *A Study of Electrical, Optical and Structure Properties of AS–Se–TI Thin Film*, Ph.D, (South Valley University, 2005)
24. M. Dongol, M.M. El-Nahass, M. Abou-zied, A. El-Denglawey, Eur. Phys. J. Appl. Phys. **37**, 257 (2007)
25. E.R. Shaaban, N. Afify, A. El-Taher, J. Alloys Compds. **482**, 400 (2009)
26. H.M. Zeyada, M.M. El-Nahass, M.M. Makhlouf, Curr. Appl. Phys. **11**, 1326 (2011)
27. R. Tellier, Thin Solid Films **51**, 311 (1978)
28. K.L. Chopra, *Thin Film Phenom.* (Mc Graw Hill, New York, 1969)
29. D. Lakshminarayana, R.R. Desai, J. Mater. Sci. Mater. Electron. **4**, 183 (1993)
30. N.F. Mott, E.A. Davis, *Electronic Processes in Non Crystalline Materials* (Clarendon Press, Oxford, 1971)
31. C.C. Regimol, C.S. Menon, Mater. Sci. Pol. **25**, 649 (2007)
32. A.K. Hassan, R.D. Gould, J. Phys. Condens. Matter. **1**, 6679 (1989)
33. N.F. Mott, Philos. Mag. **22**, 7 (1970)
34. N.F. Mott, Philos. Mag. **19**, 835 (1969)
35. N.F. Mott, J. Non-Cryst. Solids **1**, 8 (1972)
36. G.B. Abdullaev, S.I. Mekhtieva, D.S. Abdinov, G.M. Aliev, Phys. Status Solid A **11**, 891 (1965)
37. A. Touraine, C. Vautier, D. Caries, Thin Solid Films **9**, 229 (1972)
38. M. Dongol, M.M. El-Nahass, M. Abou-zied, A. El-Denglawey, Phys. B **371**, 218 (2006)
39. A. Miller, E. Abrahams, Phys. Rev. **120**, 745 (1960)
40. R.M. Hill, Philos. Mag. **24**, 1307 (1971)
41. A.A. El-Shazly, D.A. El-Hady, H.S. Metwally, M.A.M. Seyam, J. Phys. Condens. Matter **10**, 5943 (1998)
42. J.S. Dugdol, *The Electrical Properties of Metals and Alloys* (Edward Arnold, London, 1979)
43. H.S. Soliman, A.M.A. El-Barry, N.M. Khosifan, M.M. El Nahass, Eur. Phys. J. Appl. Phys. **37**, 1 (2007)
44. H. Fritzsche, Solid State Commun. **9**, 1813 (1971)
45. M. Pfeiffer, A. Beyer, T. Fritz, K. Leo, Appl. Phys. Lett. **73**, 3202 (1998)
46. M.M. El-Nahass, A.M. Farid, A.A. Attia, H.A.M. Ali, Appl. Surf. Sci. **252**, 7553 (2006)
47. R. Callaerts, P. Nagels, M. Denayer, Phys. Lett. A **38**, 15 (1972)
48. P. Nagels, R. Callaerts, M. Denayerm, R. Deconinck, J. Non-Cryst. Solids **4**, 295 (1970)
49. D. Emin, C.H. Seager, R. Quinn, Phys. Rev. Lett. **28**, 813 (1972)
50. H.K. Rockstad, R. Flasck, S. Iwasa, J. Non-Cryst. Solids **262**, 8 (1972)
51. N.K. Hindleyn, J. Non-Cryst. Solids **5**, 17 (1970)
52. A.J. Grant, T.D. Moustakas, T. Penney, K. Weiser, in *Proceedings of the 5th International Conference on Amorphous and Liquid Semiconductors*, (Taylor and Francis, London, 1974), p. 325
53. H. Overhof, W. Beyer, Philos. Mag. B **49**, 9 (1984)
54. T.M. Donovan, K. Heinemann, Phys. Rev. Lett. **27**, 1794 (1971)
55. J.J. Hauser, A. Staudinger, Phys. Rev B. **12**, 2448 (1975)
56. J.J. Hauser, A. Staudinger, Solid State **70**, 112 (2001)
57. Z.H. Khan, M. Zulfeqaur, A. Kumar, M. Husain, Can. J. Phys. **80**, 19 (2002)